Fast Frequency Response of Distribution Feeders Equipped with CIGs: An MRAC Based Approach

F. Ahmadi *, A.M. Brambilla*, D. del Giudice*, F. Bizzarri*
* Department of Electronics, Information Technology and Bioengineering, Politecnico di Milano, Milan, Italy.
Email: {farahnaz.ahmadi, angelo.brambilla, davide.delgiudice, federico.bizzarri}@polimi.it

***Abstract*—The renewable energy source-fueled grid-following and/or grid-forming converter-interfaced generators in distribution feeders allow the provision of fast frequency response. Their contribution to this ancillary service can differ from the wanted one since converter-interfaced generators may not be always available and they are spread in the feeder, leading to different contributions to a power disturbance. To achieve the desired fast frequency response at the point of common coupling, it is necessary to implement a proper control strategy to dynamically regulate the inertia and load damping contributions by at least a subset of converter-interfaced generators. This paper proposes a strategy based on a direct model reference adaptive controller (MRAC) to achieve this target. To evaluate the performance of the proposed controller, simulation results obtained by applying it to a modified version of the IEEE 13-node feeder are presented.**

***Index Terms*—distribution feeder, fast frequency response, MRAC, virtual inertia and load damping.**

I. Introduction

The increasing penetration of renewable energy sources (RESs) such as photovoltaic and wind plants has intensified the reliance on inverter-based resources (IBRs) in modern power systems. RESs connect to the grid through power electronic converters: as such, they are hereafter referred to as converter-interfaced generators (CIGs). The absence of inherent inertia in CIGs leads to challenges in maintaining grid stability, necessitating the implementation of sophisticated control strategies to manage power sharing, voltage and frequency regulation, and overall grid resilience. To overcome these issues, CIGs controllers, which can operate in either grid-following (GFL) or grid-forming (GFM) mode [1], can be modified by letting them provide virtual inertia and load damping, in an attempt to mimic the behaviour of synchronous generators [2]–[4].

Most CIG control strategies rely on fixed values of virtual inertia and load damping. These values may not always sum up to the desired values at the point of common coupling (PCC) of feeders for two main reasons. First, CIGs may not be always available (e.g., due to a lack of primary energy source). Second, CIGs are scattered across feeders. It is thus reasonable to expect that their power response to a disturbance (which ultimately gives shape to the fast frequency response (FFR)) changes based on their location. For example, FFR may change if all CIGs were connected directly at the PCC. For this reason, adaptive control strategies have been developed, which modulate some CIG control parameters to attain a desired equivalent behavior at the PCC. Although there is an extensive research on adaptive virtual inertia of CIGs [5]–[7], only a limited number of studies have integrated both inertia and damping adaptations into their control strategies [8]–[10].

In this paper, we consider the IEEE 13-node benchmark system, modified by adding three GFM CIGs: one is assumed controllable and the others providing unknown levels of virtual inertial and load damping. We exploit a direct model reference adaptive controller (MRAC) [11], [12] to properly online tune the virtual inertia and load damping of the controllable CIG. The controller aims at adjusting those parameters in such a way the feeder provides the desired level of FFR at the PCC.

To this aim, the distribution feeder at the PCC is modeled as an equivalent *reference system* (in this case a reference *swing equation*), with predefined *desired* inertia and load damping values (say H_{R} and D_{R}, respectively), receiving as input the ΔP_{P} fluctuations (w.r.t. the power flow (PF) solution) of the electrical power flowing through the PCC. We show MRAC dynamically adjusts the parameters of the controllable CIG, without needing to know or to estimate online the inertia and load damping of the other CIGs belonging to the feeder, to make the actual ω_{P} electrical angular frequency at PCC evolving in time as close as possible to the ω_{R} angular frequency of the reference system.

II. Open-loop system model: the plant

Adaptive control offers mechanisms that adjust a controller for a system facing parametric, structural, and environmental uncertainties, ensuring the desired performance is achieved. To identify an appropriate MRAC in charge of governing online the H_{CIG} virtual inertia and the D_{CIG} load damping of at least one of the CIGs so that the corresponding feeder provides at the PCC a desired level of FFR, it is essential to establish the equations that model the system in open-loop form (the *plant*) with an acceptable level of detail. Given our focus on how a generic feeder contributes to FFR, we will assume that a typical distribution feeder can be represented by the swing equation

$$2\widehat{H}_{\mathrm{P}}\Delta\dot{\omega}_{\mathrm{P}} = \Delta P_{\mathrm{P}} - \widehat{D}_{\mathrm{P}}\Delta\omega_{\mathrm{P}} \ , \tag{1}$$

where $\Delta\omega_{\mathrm{P}}$ denotes the angular frequency variation w.r.t. the nominal value of the electric angular frequency measured at the PCC, and ΔP_{P} is the power exchange fluctuation between the feeder and the electrical grid. When ΔP_{P} is negative (positive), the feeder supplies (absorbs) active power. At steady

The work of F. Bizzarri and F. Ahmadi was partially supported by Italian MUR under the grant PRIN 2022 DCNanoSyn, CUP D53D23001500006, project code 2022SPFP9R.

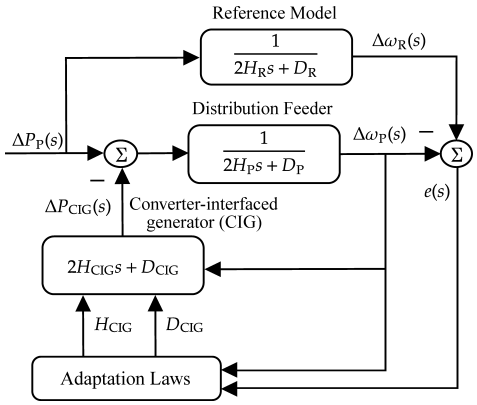

Fig. 1: The proposed MRAC scheme.

state (i.e., the PF solution), $\Delta P_{\rm P} = 0$. In Eq. (1), $\widehat{H}_{\rm P}$ and $\widehat{D}_{\rm P}$ denote the *equivalent desired* inertia and load damping constants, respectively. $\widehat{H}_{\rm P}$ and $\widehat{D}_{\rm P}$ depend on the virtual inertia and load damping constants of the CIGs of the feeder. As already said, these values do not simply sum up the corresponding ones of the CIGs connected to the feeder buses. It is thus impossible to express in closed form how these individual contributions combine to form the equivalent $H_{\rm P}$ and $D_{\rm P}$ at the PCC.

An exception arises if we assume to have only one CIGs directly connected at the PCC, thus working "in parallel" with the distribution feeder. We write its contribution to FFR as[1]

$$\Delta P_{\rm CIG} = 2H_{\rm CIG}\Delta\dot{\omega}_{\rm CIG} + D_{\rm CIG}\Delta\omega_{\rm CIG} \ . \tag{2}$$

Since $\Delta\omega_{\rm CIG} \approx \Delta\omega_{\rm P}$, by ignoring the contribution of this specific CIG, if we now assume that the uncertain inertia and load damping constants of the equivalent feeder model are $H_{\rm P}$ and $D_{\rm P}$, respectively, $\Delta P_{\rm CIG}$ and $\Delta P_{\rm P}$ directly sum up as

$$2H_{\rm P}\Delta\dot{\omega}_{\rm P} = \Delta P_{\rm P} - \Delta P_{\rm CIG} - D_{\rm P}\Delta\omega_{\rm P} \ , \tag{3}$$

Through (2), Eq. (3) can be recast as

$$2(H_{\rm P} + H_{\rm CIG})\Delta\dot{\omega}_{\rm P} = \Delta P_{\rm P} - (D_{\rm P} + D_{\rm CIG})\Delta\omega_{\rm P} \ . \tag{4}$$

Keeping in mind that $H_{\rm P}$ and $D_{\rm P}$ are *uncertain* parameters, we aim at regulating $H_{\rm CIG}$ and $D_{\rm CIG}$ to have

$$H_{\rm P} + H_{\rm CIG} = \widehat{H}_{\rm P} \quad \text{and} \quad D_{\rm P} + D_{\rm CIG} = \widehat{D}_{\rm P}. \tag{5}$$

Said in another way, given the already *unknown* $H_{\rm P}$ and $D_{\rm P}$ contributions, we would like to set $H_{\rm CIG}$, $D_{\rm CIG}$ to obtain the *desired* $\widehat{H}_{\rm P}$ and $\widehat{D}_{\rm P}$ contributions at the PCC.

III. Adaptive inertia and damping control design

The block diagram of the proposed direct MRAC scheme is shown in Fig. 1. Hereafter, its design is presented in detail.

[1]This assumption is not realistic and it will be removed in the case study presented in Sec. IV.

A. Reference Model Selection

MRAC systems aim at updating the parameters of the control law so that the behavior of the resulting system becomes as close as possible to that of a given *reference model*. Since (4) is a first-order dynamical system, a reference model with the same structure is chosen:

$$2H_{\rm R}\Delta\dot{\omega}_{\rm R} = r - D_{\rm R}\Delta\omega_{\rm R} \ , \tag{6}$$

where, $H_{\rm R}$, $D_{\rm R}$, and $\Delta\omega_{\rm R}$ represent the inertia constant, load damping coefficient, and frequency variation of the desired reference model, respectively. The r *command signal* of the *reference model*, corresponds to $\Delta P_{\rm P}$ in (4). Defining $a_{\rm r} = -D_{\rm R}/2H_{\rm R}$ and $b_{\rm r} = 1/2H_{\rm R}$, (6) reduces to

$$\Delta\dot{\omega}_{\rm R} = a_{\rm r}\Delta\omega_{\rm R} + b_{\rm r}r \ . \tag{7}$$

B. Controller Structure Determination

Consider the following proportional-derivative (PD) controller structure, which is designed to enable the closed-loop system to accurately follow a control input

$$u = k_{\rm d}\Delta\dot{\omega}_{\rm P} + k_{\rm p}\Delta\omega_{\rm P} + k_{\rm r}r \ , \tag{8}$$

where $k_{\rm d}$ and $k_{\rm p}$ are the adjustable derivative and proportional gains of the PD controller in the feedback path, and $k_{\rm r}$ is the fixed feed-forward gain.

By considering (2) and by assuming $a_{\rm p} = -D_{\rm P}/2H_{\rm P}$ and $b_{\rm p} = 1/2H_{\rm P}$, Eq. (3) can be rewritten as

$$\Delta\dot{\omega}_{\rm P} = a_{\rm p}\Delta\omega_{\rm P} + b_{\rm p}u \ , \tag{9}$$

where

$$u = -2H_{\rm CIG}\Delta\dot{\omega}_{\rm P} - D_{\rm CIG}\Delta\omega_{\rm P} + \Delta P_{\rm P} \ . \tag{10}$$

By comparing the control signal in (8) and (10), we have

$$k_{\rm d} = -2H_{\rm CIG}, \quad k_{\rm p} = -D_{\rm CIG}, \quad k_{\rm r} = 1, \quad r = \Delta P_{\rm P} \ .$$

We underline that, contrary to a canonical MRAC architecture, that in Fig. 1 exhibits a peculiarity: typically r is an exogenous signal feeding the plant and the reference system. Here this is not the case because $\Delta P_{\rm P}$ is altered by the controlling action that adjusts $H_{\rm CIG}$ and $D_{\rm CIG}$. Since the plant is connected at the PCC to the electrical grid, which influences its dynamical evolution, $\Delta P_{\rm P}$ cannot be considered as if it were an independent and external command signal. This is basically the reason why we must choose $k_{\rm r} = 1$ (i.e., the feed-forward gain cannot be freely set to enforce the desired control strategy).

At first, the ideal controller

$$u^* = k_{\rm d}^*\Delta\dot{\omega}_{\rm P} + k_{\rm p}^*\Delta\omega_{\rm P} + r \ ,$$

is defined to fully compensate for uncertainties, ensuring that $\Delta\omega_{\rm P}$ precisely tracks $\Delta\omega_{\rm R}$. By comparing the ideal closed-loop plant with the reference model, the ideal gains can be obtained using model-matching conditions

$$k_{\rm d}^* = \frac{b_{\rm r} - b_{\rm p}}{b_{\rm p}b_{\rm r}}, \quad k_{\rm p}^* = \frac{b_{\rm p}a_{\rm r} - a_{\rm p}b_{\rm r}}{b_{\rm p}b_{\rm r}} \ . \tag{11}$$

C. Adaptation Mechanisms Design

The proposed MRAC is designed using a Lyapunov-based approach, ensuring the stability of the closed-loop system. The tracking error is

$$e = \Delta\omega_{\mathrm{R}} - \Delta\omega_{\mathrm{P}} \ . \tag{12}$$

The objective is to design a controller for (9) that guarantees e converges to zero asymptotically, even when H_{P} and D_{P} are uncertain. The error dynamics is obtained through (7) – (9)

$$\dot{e} = a_{\mathrm{r}} e - b_{\mathrm{r}} \widetilde{k}_{\mathrm{d}} \Delta\dot{\omega}_{\mathrm{P}} - b_{\mathrm{r}} \widetilde{k}_{\mathrm{p}} \Delta\omega_{\mathrm{P}} \ , \tag{13}$$

where $\widetilde{k}_{\mathrm{d}} = k_{\mathrm{d}} - k_{\mathrm{d}}^*$ and $\tilde{k}_{\mathrm{p}} = k_{\mathrm{p}} - k_{\mathrm{p}}^*$ are the estimation errors. The adaptive laws for adjusting k_{d} and k_{p} are derived by exploiting the Lyapunov stability approach, obtaining [13]

$$\begin{aligned} H_{\mathrm{CIG}}(t) &= -\tfrac{1}{2}\gamma_{\mathrm{d}} \int_0^t e(\tau)\Delta\dot{\omega}_{\mathrm{p}}(\tau)d\tau + H_{\mathrm{CIG}}(0) \\ D_{\mathrm{CIG}}(t) &= -\gamma_{\mathrm{p}} \int_0^t e(\tau)\Delta\omega_{\mathrm{p}}(\tau)d\tau + D_{\mathrm{CIG}}(0) \, , \end{aligned} \tag{14}$$

where γ_{d} and γ_{p} are the adaptation rates of the derivative and proportional gain, respectively.

We underline that, according to the assumption that the controlled CIG is connected at the PCC in parallel with the feeder, (14) will provide the values of the parameters to be used in (5) to attain the desired values of inertia and load damping at the PCC. They correspond to $H_{\mathrm{CIG}} = \widehat{H}_{\mathrm{P}} - H_{\mathrm{P}}$ and $D_{\mathrm{CIG}} = \widehat{D}_{\mathrm{P}} - D_{\mathrm{P}}$ (recall that both H_{P} and D_{P} are considered uncertain parameters and for this reason we used and adaptive controller). In practice, and in particular in the case study considered in Sec. IV, the controlled CIG is *not* connected at the PCC. The MRAC will provide H_{CIG} and D_{CIG} different values from those in (5); the value of these parameters will be chosen by the controller in such a way that at the PCC the overall feeder is as much as possible "equivalent" to the swing equation characterized by $\widehat{H}_{\mathrm{P}}$ and $\widehat{D}_{\mathrm{P}}$.

IV. Simulation Results

The proposed MRAC was tested by exploiting the modified version of the IEEE 13-node test feeder in Fig. 2 [14]. The benchmark is of small scale and characterized by relatively highly unbalanced loads, a single voltage regulator at the substation, overhead and underground lines, shunt capacitors, and an in-line transformer. We adopted the grid model available from the MATLAB simulation platform [15] in the Simscape™ Electrical™ Specialized Power Systems toolbox[2] for the simulations. With respect to its original version, that shown in Fig. 2 has additional elements highlighted in **violet**. Among those, there is a 100 MVA synchronous generator connected to node 632 through a transmission line and a proper power transformer added to step down the voltage from 15 kV at the generator output to the 4.16 kV of the feeder. The L_2 load is purely resistive and absorbs 20 MW per phase. We

[2]The original MATLAB model is available at https://it.mathworks.com/help/sps/ug/ieee-13-node-test-feeder.html where the reader can find out the values of all the parameters. In case of acceptance of the manuscript, the Authors will make available the simulation files on a GitHub repository.

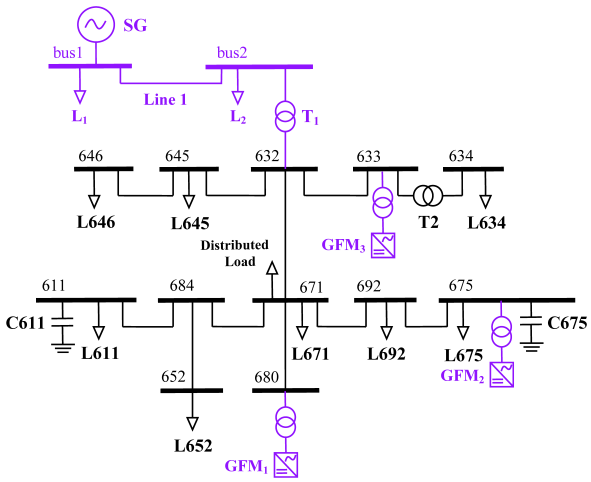

Fig. 2: The modified IEEE 13-node test feeder: extra elements are shown in violet. The per-unit length parameters of Line 1, which is 6.1 km long, are the same of the line connecting node 632 and 671.

also connected GFM CIGs at nodes 680, 675, and 633: their nominal capacity is 10 MVA. The active power set-point of GFM_1 is 3 MW, whereas that of GFM_2 and GFM_3 is fixed to 1.5 MW. The reactive power set-point of all of them is null. We assume that their internal controllers have infinite bandwidth compared to the relatively slower process of power system frequency regulation. So doing, GFM CIGs are modeled as a basic swing equation.

To trigger frequency variations and assess the effectiveness of MRAC, a power disturbance is needed. This is attained by acting on the power profile of the L_1 resistive load. This load is fixed at 3.5 MW at PF and varies as a square-wave of period 20 s and 50% duty-cycle, alternating between 7 MW and 0 MW during time domain simulations. The choice of selecting this kind of power disturbance to let the MRAC adjust the CIG inertia and load damping can be justified as follows:

- applying a periodic profile excites the system across a wider frequency range, yielding more detailed insights into its dynamic characteristics;
- a periodic input promotes continuous and steady parameter updates, which helps achieve quicker convergence;

Contrary to GFM_2 and GFM_3, GFM_1 is equipped with a MRAC. In the absence of any control, the H_1 inertia and D_1 load damping coefficients of GFM_1 are fixed at 2 s and 5, respectively. These are the only values that are assumed to be known, viz. no information is directly available to concerning GFM_2 and GFM_3. H_1 and D_1 contribute to a_{p} and b_{p}. Of course, the latter are not the actual values for the plant, but they represent a guess according to the information available at the beginning of the analysis. Under the assumptions that we aim at achieving $H_{\mathrm{R}} = 15\mathrm{s}$ and $D_{\mathrm{R}} = 35$, we derive k_{d}^* and k_{p}^*. The action of the MRAC, dynamically varies H_1 and D_1 by summing H_{CIG} and D_{CIG}, respectively, which are computed according to (14) ($\gamma_{\mathrm{p}} = 10^5$ Hz and $\gamma_{\mathrm{d}} = 10^6$ s). From k_{d}^* and k_{p}^*, we have $H_{\mathrm{CIG}}(0) = 13$ s and $D_{\mathrm{CIG}}(0) = 30$. The adaptive controller is turned on at $t = 0$ when the

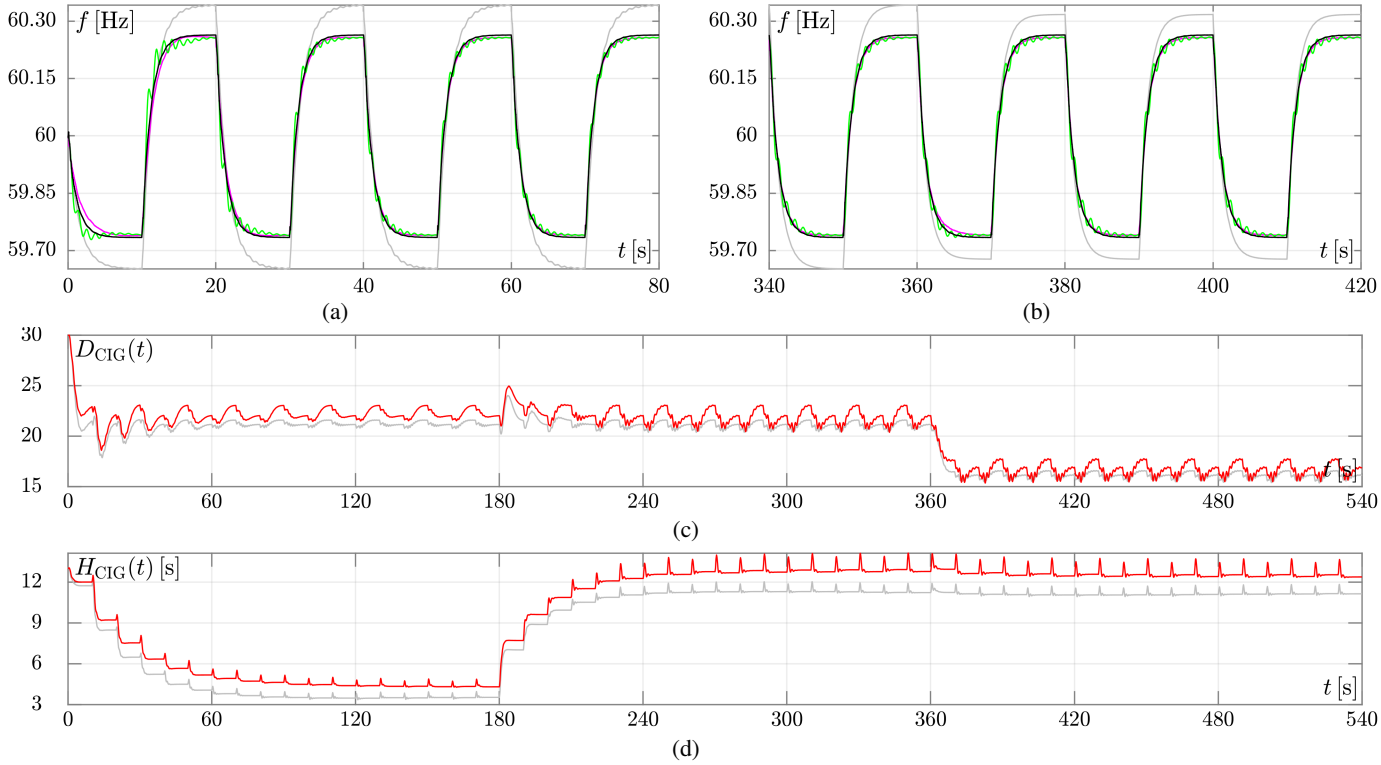

Fig. 3: (a-b) Frequency response at the PCC under a periodic variation of L_1 in Fig. 2. The green curve represents the reference model, while the magenta and gray curves depict the results with and without MRAC, respectively. The black curve refers to the case where a single equivalent CIG (nominal capacity 10 MVA) with inertia and load damping coefficients fixed to $H_{\mathrm{R}} = 15\,\mathrm{s}$ and $D_{\mathrm{R}} = 35$, respectively, is connected at the PCC. D_{CIG} and H_{CIG} evolution due to the proposed MRAC are reported in gray in (c) and (d), respectively. The red curves refer to the case in which the line between node 671 and 680 is five times longer than in the reference case.

first step variation of L_1 occurs. During the evolution of the system, MRAC must compensate through the action of GFM_1 the presence of GFM_2 and GFM_3. In this case study, we chose $H_3 = 2\,\mathrm{s}$ and $D_3 = 5$, whereas H_2 and D_2 vary in time. In particular, $D_2 = 5$ for $t < 360\,\mathrm{s}$ and then jumps to 10. Similarly, $H_2 = 8\,\mathrm{s}$ for $t < 180\,\mathrm{s}$ and then jumps to $0.5\,\mathrm{s}$.

The gray line in Fig. 3(a-b) shows the frequency response at the PCC due to the L_1 load power variation when the MRAC is not present and the CIGs within the feeder provide their default value of virtual inertia and load damping. Panel (a) shows the first part of the simulation whereas panel (b) highlights the effect of the jump in the D_2 damping coefficient. The green curve shows the frequency evolution of the reference model fed by ΔP_{P}, while the magenta curve refers to the frequency at the PCC when the MRAC operates. The magenta curve get very close to the green one in less than $80\,\mathrm{s}$.

To verify that the action of the MRAC is coherent with its assignment, we performed a simulation where the three CIGs are replaced by a single CIG connected directly at the PCC with an active power set-point fixed at 6 MW, a null reactive power set-point, and its inertia and load damping constants set at H_{R} and D_{R}, respectively. So doing, this is the only device connected at the PCC able to contribute to FFR. In this working condition, the evolution of the frequency at the PCC is depicted by the black curve in Fig. 3(a-b). It is worth noting that it evolves as the reference model, thus confirming a proper action of the MRAC.

The evolution of H_{CIG} and D_{CIG}, according to the action of the MRAC, is shown in Fig. 3(c-d). We see that the convergence of the frequency at the PCC to the frequency of the reference model requires a variation of H_{CIG} and D_{CIG} w.r.t. to their initial values. Once convergence is achieved before the step of H_2 at $180\,\mathrm{s}$, the overall inertia and damping provided by the CIGs are approximately $15.5\,\mathrm{s}$ and 36, respectively. This means that, in order to make the feeder working at the PCC as the reference model, it is not possible to simply distribute H_{R} and D_{R} between the CIGs. To confirm it, we performed the same simulation but making the line between node 671 and 680 five times longer than in the reference case. It can be noticed (see the red curves in Fig. 3(c-d)) that H_{CIG} and D_{CIG} varies w.r.t. the original simulation.

V. Concluding Remarks

We detailed the design of a model reference adaptive controller (MRAC) operating in closed-loop configuration to suitably govern the virtual inertia and load damping parameters of a GFM CIG connected to an *internal* node of a feeder (far from the PCC) to guarantee the desired level of virtual inertia and load damping at the feeder sub-station (PCC). Simulations show it works properly and sets the GFM parameters in a relatively short time interval (less than $100\,\mathrm{s}$).

REFERENCES

[1] N. Mohammed, W. Zhou, B. Bahrani, and D. J. Hill, "Support vector machines for predicting the impedance model of inverter-based resources," *IEEE Trans. on Power Systems*, vol. 39, no. 6, pp. 7359–7375, 2024.

[2] H.-P. Beck and R. Hesse, "Virtual synchronous machine," in *2007 9th International Conference on Electrical Power Quality and Utilisation*, 2007, pp. 1–6.

[3] S. D'Arco and J. A. Suul, "Equivalence of virtual synchronous machines and frequency-droops for converter-based microgrids," *IEEE Trans. on Smart Grid*, vol. 5, no. 1, pp. 394–395, 2014.

[4] A. M. Brambilla, D. d. Giudice, and F. Bizzarri, "Improved stability of a grid-following converter controller supplying virtual inertia and damping," *IEEE Trans. on Power Delivery*, vol. 40, no. 2, pp. 900–911, 2025.

[5] M. Ren, T. Li, K. Shi, P. Xu, and Y. Sun, "Coordinated control strategy of virtual synchronous generator based on adaptive moment of inertia and virtual impedance," *IEEE Journal on Emerging and Selected Topics in Circuits and Systems*, vol. 11, no. 1, pp. 99–110, 2021.

[6] G. W. Chang and K. T. Nguyen, "A new adaptive inertia-based virtual synchronous generator with even inverter output power sharing in islanded microgrid," *IEEE Trans. on Industrial Electronics*, vol. 71, no. 9, pp. 10 693–10 703, 2024.

[7] X. Hou, Y. Sun, X. Zhang, J. Lu, P. Wang, and J. M. Guerrero, "Improvement of frequency regulation in VSG-based AC microgrid via adaptive virtual inertia," *IEEE Trans. on Power Electronics*, vol. 35, no. 2, pp. 1589–1602, 2020.

[8] D. Li, Q. Zhu, S. Lin, and X. Y. Bian, "A self-adaptive inertia and damping combination control of VSG to support frequency stability," *IEEE Trans. on Energy Conversion*, vol. 32, no. 1, pp. 397–398, 2017.

[9] E. Gurski, R. Kuiava, F. Perez, R. A. Benedito, and G. Damm, "A novel VSG with adaptive virtual inertia and adaptive damping coefficient to improve transient frequency response of microgrids," *Energies*, vol. 17, no. 17, p. 4370, 2024.

[10] U. Markovic, Z. Chu, P. Aristidou, and G. Hug, "LQR-based adaptive virtual synchronous machine for power systems with high inverter penetration," *IEEE Trans. on Sustainable Energy*, vol. 10, no. 3, pp. 1501–1512, 2019.

[11] F. Ahmadi, Y. Batmani, and H. Bevrani, "On design of power sharing for VSC-based islanded AC microgrids: An adaptive MIMO controller equipped with a predictor," *IET Generation, Transmission & Distribution*, vol. 17, no. 18, pp. 4161–4171, 2023.

[12] K. J. Åström and B. Wittenmark, *Adaptive control*. Courier Corporation, 2013.

[13] N. Nguyen, *Model-Reference Adaptive Control: A Primer*, ser. Advanced Textbooks in Control and Signal Processing. Springer International Publishing, 2018.

[14] K. P. Schneider, B. A. Mather, B. C. Pal, C.-W. Ten, G. J. Shirek, H. Zhu, J. C. Fuller, J. L. R. Pereira, L. F. Ochoa, L. R. de Araujo, R. C. Dugan, S. Matthias, S. Paudyal, T. E. McDermott, and W. Kersting, "Analytic considerations and design basis for the IEEE distribution test feeders," *IEEE Trans. on Power Systems*, vol. 33, no. 3, pp. 3181–3188, 2018.

[15] T. M. Inc., "MATLAB version: 24.2.0.2806996 (R2024b)," Natick, Massachusetts, United States, 2024. [Online]. Available: https://www.mathworks.com